

Evolution of the X-ray luminosity and metallicity of starburst blown superbubbles

Sergey A. Silich ¹ [★], Guillermo Tenorio-Tagle ² [†], Roberto Terlevich ³ [‡]
 Elena Terlevich ² [§] & Hagai Netzer ⁴

¹ Main Astronomical Observatory National Academy of Sciences of Ukraine, 03680, Kiev-127, Golosiv, Ukraine

² Instituto Nacional de Astrofísica Óptica y Electrónica, AP 51, 72000 Puebla, México

³ Institute of Astronomy, Madingley Road, Cambridge CB3 0HA, UK

⁴ School of Physics and Astronomy, Tel Aviv University, Tel Aviv, Israel.

1 November 2018

ABSTRACT

We calculate the time-dependent metal production expected from starbursts and use them as boundary conditions in our 2D simulations of evolving superbubbles. We assume that the produced metals (oxygen and iron) thoroughly mix with the ejected stellar envelopes, and/or with the matter thermally evaporated from the superbubble cold outer shell. The metal production process determines the time-dependent metallicity in hot superbubble interiors, and leads to values of $Z \geq Z_{\odot}$ when oxygen is used as tracer, and under-solar when the metallicity is measured with respect to iron. In either case, the enhanced metallicity boosts the X-ray emissivity of superbubbles, bringing theory and observations closer together.

Key words: ISM: abundances, ISM: bubbles, ISM: hydrodynamics, galaxies: starbursts, X-rays: bursts

1 INTRODUCTION

The formation and evolution of galaxies is one of the most captivating problems of modern astrophysics. With present-day techniques, young star clusters can be observed at large look-back times and much work has been devoted to the detailed studies of the optical and near UV properties of such systems at intermediate and high redshifts. The defining characteristic of starburst galaxies is their spectrum which is the emission lines from HII regions in extremely young (≤ 10 Myr) star forming regions. While the UV radiation from the massive stars excite and ionize the associated HII regions, the stellar winds and supernova explosions lead to giant hot bubbles in the interstellar medium (ISM).

Most of the information about the properties of the “warm ISM” in young giant star-forming regions comes from the analysis of their emission lines. Such observations indicate that the warm ISM in starburst galaxies is not yet contaminated by the metals ejected by the present burst. However, little is known about the “hot ISM”, where most of the newly produced metals are presumably located. Data

from *ROSAT*, *ASCA* and *BeppoSAX*, although inconclusive, seem to suggest sub-solar iron abundance and about solar abundances for the α -elements (Bauer & Bregman 1996, Ptak *et al.* 1999, Persic *et al.* 1998, but see Dahlem, Weaver & Heckman 1998 and Weaver *et al.* 1999). However, The abundances determined from the optical emission lines, in some of the best studied galaxies, is considerably higher than those derived from the X-ray data. This conflict is likely to be resolved soon, with the coming new high resolution spectroscopic observations of *Chandra* and *XMM*.

The mechanical energy from evolving starbursts is known to lead to the formation of superbubbles in the ISM. This happens as the violently ejected matter from winds and supernovae becomes thermalized at a reverse shock. This provides it with the high temperature ($T \geq 10^7$ - 10^8 K) and the high thermal pressure that allows it to drive a strong shock (the so called outer shock) into the surrounding ISM. The outer shock is responsible for sweeping and accelerating the surrounding gas into a large-scale shell, while the high sound speed, thermalized ejecta, fills most of the volume formerly occupied by the swept up gas. The two gases, the ejecta and the swept up ISM, are separated by a contact discontinuity and thus there is little enrichment, at this time, of the galaxy ISM (Tenorio-Tagle 1996).

Several calculations (see Tenorio-Tagle & Bodenheimer 1988, Silich & Tenorio-Tagle 1998 and references therein)

[★] RS Visitor at IoA, Cambridge

[†] Visitor IoA, Cambridge

[‡] Visiting Professor, INAOE

[§] Visiting fellow IoA, Cambridge

have shown how the growing structures may acquire a variety of shapes, depending on how the ISM is distributed. Fairly round and 8-shaped remnants are expected for a constant density medium and plane stratified atmospheres, respectively. Superbubbles are also known to blow out upon the sudden acceleration experienced when crossing supersonically a large negative density gradient. At that moment, the accelerated section of the shell of swept up matter becomes Rayleigh-Taylor unstable and fragments, while the hot superbubble interior is vented into the low density surrounding gas. The escaping material, flying with its sound speed, would then push again the outer shock to build a new and even larger shell evolving into the halos of galaxies. If the shock reaches the outskirts of galaxies with a speed larger than the escape velocity of the system, it may also establish a galactic wind. This is in fact detected in the case of some nuclear starbursts (e.g. Heckman *et al.* 1996, Tenorio-Tagle & Muñoz Tuñón 1998). The latter event is expected to have drastic consequences as all the newly processed starburst elements, originally found in the hot superbubble interior, will be channeled out of their parent galaxy into the intergalactic medium.

Superbubbles have been recognized for their large-scale expanding HI shells (Heiles 1979, Brinks & Bajaja 1986, Maschenko *et al.* 1999). Some of the youngest ones are detected at optical frequencies emanating from giant HII regions (Meaburn 1980, Heckman *et al.* 1990, Martin 1996, Oey 1996), and many have been recognized by the X-ray emitted from their hot interiors (Wang & Helfand 1991, Heckman 1995, Wang 1999).

Several authors have pointed out a large discrepancy between theory and observations of superbubbles. Current predictions are based on the fact that, in the temperature range of $\sim 10^6 - 10^7$ K, the X-ray emissivity can be approximated by a linear function of the gas metallicity. For the 0.1 - 2.4 keV energy band, this can be approximated by a constant value $\Lambda_x = 3\xi \times 10^{-23}$ erg cm³ s⁻¹, where ξ is the metallicity in solar units. A simple analytic model may then be developed to estimate the X-ray luminosity from a spherically symmetric, energy dominated bubble bound by a cold radiative shell, and presenting a self-similar temperature and density distributions (see Chu & Mac Low 1990 for a constant energy input rate, and Silich 1995 for a power-law energy deposition). For a constant ambient gas density, and constant energy input rate, the X-ray luminosity over the energy band 0.1 - 2.4 keV is given by

$$L_x = 10^{36} \xi I(\tau) L_{38}^{33/35} n_0^{17/35} t_7^{19/35} \text{erg s}^{-1}, \quad (1)$$

where L_{38} is the mechanical luminosity of the starburst in units of 10^{38} erg s⁻¹, n_0 is the ambient gas number density, and t_7 is the evolutionary time in units of 10^7 yr. $I(\tau)$ is a dimensionless integral:

$$I(\tau) = \frac{125}{33} - 5\tau^{1/2} + \frac{5}{3}\tau^3 - \frac{5}{11}\tau^{11/2}, \quad (2)$$

and $\tau = T_{cut}/T_c$ is the ratio of the X-ray cut-off temperature (or lowest limit considered for the gas temperature to lead to an important X-ray emission; $T_{cut} \approx 5 \times 10^5$ K) to the bubble central temperature.

These simple considerations have been applied to a number of objects, from stellar wind bubbles to starburst galaxies. In many cases, the observed X-ray luminosities are

in clear disagreement with the model predictions and exceed, by much, the model predictions (e.g. Chu & Mac Low, 1990 for LMC bubbles; Walter *et al.*, 1998 for a superbubble in the nearby dwarf galaxy IC 2574; Martin & Kennicutt, 1995 for diffuse X-ray emission from the central region of the starburst galaxy NGC 5253). There are several proposed solutions. Chu & Mac Low (1990) have proposed off-centered supernova explosions. Franco *et al.* (1993) included the interaction of a fragmented ejecta with the outer shell and Martin & Kennicutt (1995) concluded that cloud evaporation may be a dominant mechanism to increase the X-ray emission.

Here we take the model one step further and show that the injection of energy and mass from an aging stellar cluster not only leads to the large-scale evolving superbubbles detected at a variety of frequencies, but also to a time-dependent enhanced metallicity of their hot interior. Section 2 discusses the time dependent production of metals released within the hot superbubble interior. Section 3 presents the calculations of the energy deposited by massive coeval starbursts and the implications regarding the cooling of the gas and the mixing of the enriched material. The resultant time-dependent X-ray luminosity, is given in section 4 and some conclusions are drawn in section 5.

2 TIME-DEPENDENT METAL PRODUCTION IN STARBURSTS

We assume that the total amount of gas ejected by supernovae (SNe) includes an important fraction of newly synthesized oxygen and iron, and that the extended stellar outer envelope has the same metallicity as the host galaxy ISM. We further assume that the matter violently ejected by SN as a starburst evolves is efficiently thermalized at a reverse shock and well mixed with the gas that evaporates from the cold radiative shell segments. However, a contact discontinuity inhibits its immediate mixing with the ISM, which is rapidly removed and accelerated by the outer shock (Tenorio-Tagle 1996). Consequently, the metals ejected by sequential SNe are to be found in the “hot cavity” or superbubble interior, causing drastic changes to its metallicity.

We assume a Salpeter stellar initial mass distribution (IMF)

$$n(m) = f_0 m^{-\alpha}, \quad (3)$$

within a range of upper $M_{up} = 100M_\odot$ and lower $M_{low} = 1M_\odot$ cut-off masses and a slope of $\alpha = 2.35$. The normalization constant f_0 is determined by the total mass of the star cluster M_{SB} ,

$$f_0 = \frac{(\alpha - 2)M_{SB}}{M_{low}^{2-\alpha} - M_{up}^{2-\alpha}}. \quad (4)$$

Assuming for simplicity that massive stars loose *all their mass* as they explode as SNe (Pilyugin 1992, Pilyugin & Edmunds 1996), we find the total ejected mass as a function of the cluster age t ,

$$M_{ej}(t) = f_0 \int_{M_*(t)}^{M_{up}} m^{1-\alpha} dm = M_{SB} \frac{M_*(t)^{2-\alpha} - M_{up}^{2-\alpha}}{M_{low}^{2-\alpha} - M_{up}^{2-\alpha}}, \quad (5)$$

where the mass of the stars exploding after an evolutionary time t , ($M_*(t)$), has been found using Chiosi *et al.* (1978)

and Stothers (1972) approximations to the main sequence lifetime of massive stars:

$$M_*(t) = \begin{cases} 10(9 \times 10^6/t)^2 M_\odot, & \text{for } 30M_\odot \leq M_* \leq 100M_\odot \\ 10(3 \times 10^7/t)^{5/8} M_\odot, & \text{for } 7M_\odot \leq M_* \leq 30M_\odot. \end{cases} \quad (6)$$

Heavy element yields from massive stars have been considered in a number of papers (e.g. Renzini *et al.* 1993). However, the exact values depend strongly on the adopted stellar evolution models. A recent attempt to incorporate heavy elements injection into hydrodynamical bubble models, by D'Ercole & Brighenti (1999), has included only averaged values. We have decided to consider several possible scenarios. The oxygen yield as a function of the stellar-mass (M_*) can be approximated by two different tracks: one is the "no wind" (NW) Pilyugin & Edmunds (1996) analytic approximation to Maeder (1992) and Thielemann *et al.* (1993) models for the yield

$$Y_O(M) = 0.094(M - 10.5)^{1.272} M_\odot, \quad (7)$$

which neglects the oxygen yield for stars with a mass smaller than $10.5 M_\odot$. The second "with wind" (WW) approximation, follows from stellar evolution models accounting for stellar winds (Maeder 1992, Woosley *et al.* 1993). In this case equation (7) can be used within the $10.5M_\odot \leq M_* \leq 25M_\odot$ range, assuming a constant yield up to the upper mass limit $M_{up} = 100M_\odot$.

The long term iron contamination comes mainly from the SNIa, which produce $0.5\text{--}0.7 M_\odot$ of iron after the ^{56}Ni decay. However, we are interested here in the earlier stages of the starburst evolution and thus the iron yield from the SNIa has not been taken into account. The iron production from type II SN is highly uncertain (see Renzini *et al.* 1993) and, therefore, we have considered two extreme models: Arnett (1991) and Thielemann *et al.* (1992). In the Arnett (1991) model, the iron yield increases with the mass of the star, and can be approximated by a linear function for stars between $10M_\odot \leq M_* \leq 40M_\odot$.

$$Y_{Fe}(M_*) = 0.02 + 0.006(M_* - 10) M_\odot, \quad (8)$$

For other stellar masses we have assumed constant values of Y_{Fe} . $Y_{Fe} = 0.02 M_\odot$, for $M_* \leq 10M_\odot$, and $Y_{Fe} = 0.2 M_\odot$ for $M_* > 40M_\odot$. In Thielemann *et al.* (1992), the iron yield is approximated by the exponential function

$$Y_{Fe}(M_*) = \frac{0.423}{\exp[0.31(M_* - 10.5)]} + 0.045 M_\odot, \quad (9)$$

within the $13M_\odot$ - $25M_\odot$ range, and assumed to be constant outside this range and equal to $Y_{Fe}(M_*) = 0.24 M_\odot$ for low mass stars, and $Y_{Fe}(M_*) = 0.05 M_\odot$ for stars with an initial mass larger than $25 M_\odot$. We shall refer to the above approaches for deriving the iron production rates as A (for Arnett 1991), and T (for Thielemann *et al.* 1992), respectively.

We have also assumed that the stellar matter ejected before the first SN explosion (~ 3 Myr) has the same metallicity as the ISM (see table 1). Note that the expressions used for the yields are for solar metallicity stars (which are the ones available) while the stars in the models have metallicities of $0.1 Z_\odot$. In what follows, the integrated metal content of superbubbles is given in solar values for which $Z_O = 0.0083$ and $Z_{Fe} = 0.00126$ (Grevesse, Noels & Sauval 1996).

The metallicities of the hot bubble interior relative to solar are given by

$$Z_{hot,O} = \frac{M_{ej,O}/Z_O + Z_{ISM}M_{ev}}{M_{ev} + M_{ej}}, \quad (10)$$

$$Z_{hot,Fe} = \frac{M_{ej,Fe}/Z_{Fe} + Z_{ISM}M_{ev}}{M_{ev} + M_{ej}}, \quad (11)$$

where M_{ev} is the mass added to the shocked wind region due to the cold outer shell evaporation.

Figure 1 shows the time dependent total amount of matter injected into the superbubble interior (M_{ejecta}) as a consequence of type II supernova for the NW and A approximations and the WW and T assumptions (panels a and b, respectively). This is to be compared with the total amount of oxygen (M_O) and iron (M_{Fe}) produced by the star cluster during the first 40 Myr of evolution. Note that at this time the amount of iron has not yet reached its final value, as an important contribution is expected later on from stars with a mass smaller than $10 M_\odot$.

3 SUPERBUBBLES EVOLUTION

We have carried out calculations in order to find the impact that the metals ejected by a $10^6 M_\odot$ coeval starburst may have on the ISM of galaxies with low metallicity ($Z \sim 0.1 Z_\odot$). The calculations were carried out with our three dimensional Lagrangian code, based on the thin layer approximation (Bisnovatyi-Kogan & Silich 1995, Silich & Tenorio-Tagle 1998). In all cases the total mass of the host galaxy amounts to $10^{10} M_\odot$, while the gas mass amounts only to $10^9 M_\odot$. The galaxy model was approximated with a similar prescription to that used by Li & Ikeuchi (1992), Tomisaka & Bregman (1993), Silich & Tenorio-Tagle (1998) and Tenorio-Tagle *et al.* (1999; hereafter paper I). The gas density distribution allows for two isothermal components. One is related to a central dense molecular disk with a mass of $5 \times 10^7 M_\odot$ and the second represents the low density, extended neutral halo. Both components are in a quasi-equilibrium state supported by rotation and random gas motions with a velocity dispersion of 20 and 80 km s^{-1} , respectively. The temperature of both components is $\sim 1000 \text{ K}$.

The assumed initial density distribution of the model (Figure 2) is similar to that of case A1 in Paper I. Despite its large column density ($\sim 10^{23} \text{ cm}^{-2}$) only a small fraction of this mass arises from the extended halo, and most of the undisturbed column density is within the dense molecular core. The $10^6 M_\odot$ starburst was assumed to produce a constant mechanical energy at a rate of $\sim 3.2 \times 10^{40} \text{ erg s}^{-1}$ (see Leitherer & Heckman 1995 synthesis models for low metallicity starbursts) for the first 40 Myr of its evolution, leading to a giant evolving superbubble. Three different cases are presented. In all we assume that the supernova products (oxygen and iron) rapidly mix with all the gas within the superbubble interior. As discussed in section 2, two different metal production rates, for both oxygen and iron were used, and their possible impact is discussed here and in section 4.

Case 1 follows the amount of mass thermally evaporated from the cold shell segments and considers its mixing with the ejecta from type II supernovae. The NW and A

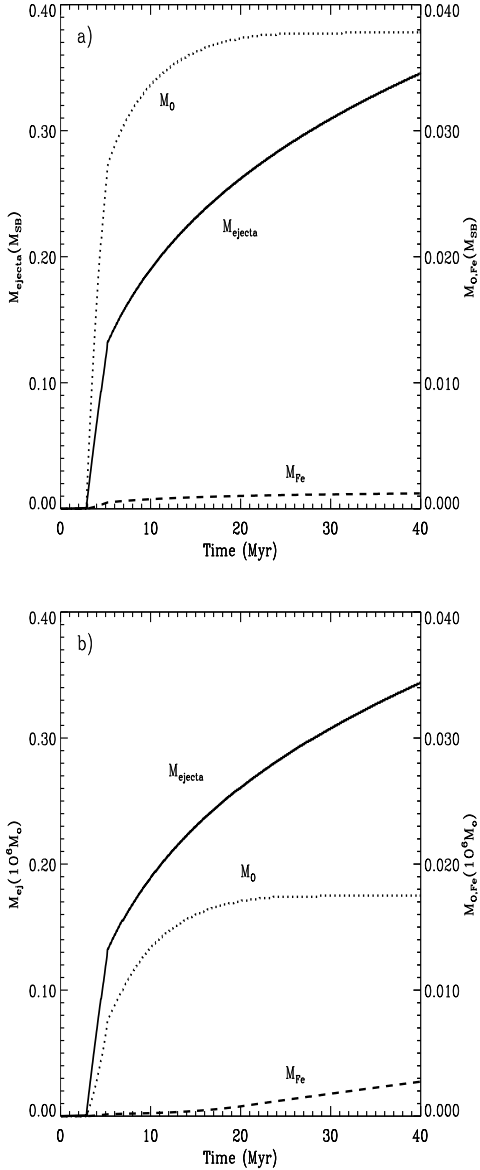


Figure 1. Time-dependent metal production from starbursts. The panels display the cumulative amount of matter (in units of the starburst mass M_{SB}) ejected by SNe as a coeval starburst evolves in time (solid line). Also shown are the amounts corresponding to oxygen (dotted lines) and to iron (dashed lines). **(a)** The oxygen production values were derived under the NW assumption and those for iron following the A approximation. **(b)** The corresponding values assumed the WW and the T approximations for oxygen and iron, respectively. The right hand side ordinate indicates the mass of O or Fe in units of the starburst mass

approximations were used for case 1A, and the WW and T approximations, for case 1B. Case 2 neglects the process of thermal evaporation and thus the metals are allowed to mix only with the ejected stellar envelopes, the latter assumed to have the same metallicity as the ISM in the host galaxy. This calculation leads to the largest metal rich superbubbles. Case 3 is almost identical to case 1, with the exception that the assumed mechanical energy input rate is

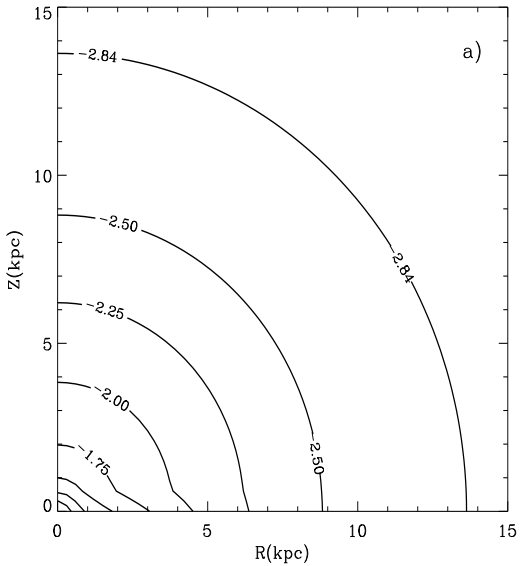


Figure 2. The logarithmic density distribution for a $10^9 M_{\odot}$ ISM model. Labels correspond to the densities and the outer contour represents the edge of the galaxy.

the one expected from a $10^7 M_{\odot}$ coeval starburst ($3.2 \times 10^{41} \text{ erg s}^{-1}$) instead of the previous $10^6 M_{\odot}$ ones. Case 3A follows the bubble evolution within a low metallicity ISM ($Z=0.1 Z_{\odot}$), whereas case 3B assumes solar metallicity for the host galaxy ISM. The model input parameters are summarized in Table 1.

The calculations follow the change of the metallicity in the superbubble interior with time and apply the correspondingly modified cooling rates. For the outer shell we assumed that its metallicity remains constant in time and equal to Z_{ISM} . The results are compared to our case A1 from paper I, which assumed that the cooling function, scaled to the initial metallicity of the host galaxy, remained unchanged with time, despite the obvious injection of new metals into the superbubble interior. Furthermore, our comparison case A1 also assumed, as in most calculations in the literature, that the same cooling function could be applied throughout the flow.

Figures 3a and 3b, show the evolution with time of the size and expansion velocity of the superbubble for cases 1A and 3A, respectively. The figure displays values of the fastest expansion velocity measured along the symmetry axis, as well as of the largest radius acquired by the superbubble during the first 40 Myr of evolution. The maximum expansion velocity shows an initial deceleration, followed by a strong acceleration that leads to several hundreds of km s^{-1} immediately after blow-out from the central disk. This short phase is abruptly interrupted once sufficient halo matter has been swept into the expanding shell causing, once again, a steady deceleration of the remnants. The maximum expansion speed is to be compared with the escape velocity from the host galaxy (V_{esc}), to discern whether the decelerating remnant remains bound (as in case 1) or is to reach the galaxy outer boundary and eject its contents into the intra-cluster medium (as in the more energetic case 3). The results of cases 1, 2 and those of case A1 of paper I are identical, as

Table 1. Model parameters

Model	L_{SB} erg s $^{-1}$	Y_O	Y_{Fe}	Z_{ISM} Z_\odot	Shell evap.
1A	3.2×10^{40}	NW	A	0.1	yes
1B	3.2×10^{40}	WW	T	0.1	yes
2A	3.2×10^{40}	NW	A	0.1	no
2B	3.2×10^{40}	WW	T	0.1	no
3A	3.2×10^{41}	NW	A	0.1	yes
3B	3.2×10^{41}	NW	A	1.0	yes
A1	3.2×10^{40}	-	-	0.1	yes

all three assumed the same mechanical energy injection and the same galaxy. The generated remnants, in all three, have identical size, expansion speed and total amount of swept-up mass. Below we show that, on the other hand, the total luminosity and the metal content inside the superbubble, are different for the different models.

The results for cases 1A and 2A are shown in Figure 4. The diagram shows the amount of matter swept by the outer shock (M_{shell}), and the mass of thermally evaporated gas from the outer shell that is ejected by supernovae (M_{hot}) (all of which is to be found in the hot superbubble interior) as a function of time. Also shown are the cumulative amounts of matter ejected by SNe (M_{ejecta}) and the corresponding amounts of oxygen (M_O) and iron (M_{Fe}). The sharp M_{shell} decrease observed at about 5 Myr results from the outer shock merging at the mid-plane of the galaxy (see Silich & Tenorio-Tagle 1998).

In case 1 (Figure 4a), the injected metals were allowed to mix thoroughly with the matter evaporated from the expanding shell. Note that for such a massive starburst, the amount of hot matter evaporated from the shell reaches a large proportion of the total mass of the shell ($M_{hot} \sim 10\% M_{shell}$). The total oxygen mass surpasses the $10^4 M_\odot$ value while the total mass in iron is $\sim 10^3 M_\odot$.

Case 2 (Figure 4b) assumes no mass evaporation from the shell, and thus apart from the small contribution due to the early wind phase, the amount of M_{hot} is very similar to the matter ejected by supernovae (M_{ejecta}). Thus the amount of oxygen and iron are very close to the values expected from the synthesis caused by the massive starburst.

Figure 5 shows the evolution of metallicity of the superbubble interior as a function of time for the different model assumptions regarding the yields, the mixing of heavy elements and the mass evaporation. Case 1A (using the NW and A approximations) rapidly (between 4 - 5 Myr) reaches over solar metalicities $Z_O \sim 8 Z_\odot$ for oxygen, and solar values for the iron tracer (Z_{Fe}) (Figure 5a). Z_O then slowly decays to about $3 Z_\odot$ after 10 Myr of evolution, to solar after 20 Myr and to under solar ($\sim 0.5 Z_\odot$) at the end of the calculation. Z_{Fe} becomes under solar after 6 Myr and slowly approaches the metallicity of the host galaxy ($0.1 Z_\odot$). The metallicity that results from case 1B, assuming the WW and T approximations for the production of metals (Figure 5b), reaches $Z_O \sim 2 Z_\odot$ after 6 Myr of evolution, falling below solar metallicity just after 10 Myr to slowly approach 0.1 Z_\odot at the end of the calculation. Z_{Fe} on the other hand, hardly shows a significant variation in this case and remains under solar throughout the calculation.

Case 2 (without mass evaporation) reaches, within short

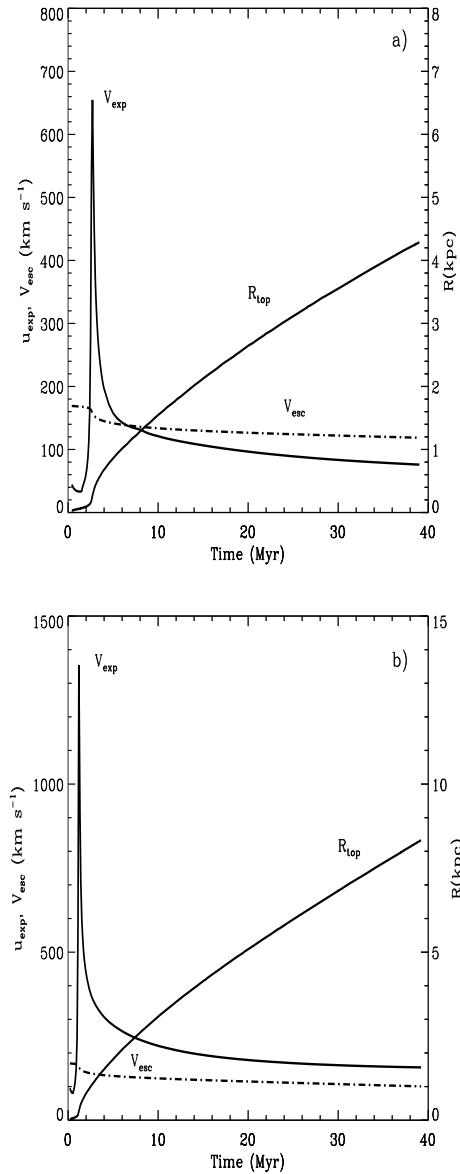


Figure 3. Evolution of the superbubbles. (a) Case 1A and (b) case 3A; shown as a function of time are the maximum expansion speed (km s $^{-1}$) measured along the symmetry axis (solid lines), the galaxy escape velocity (dash-dotted lines) and the radius (in kpc) reached by the superbubble.

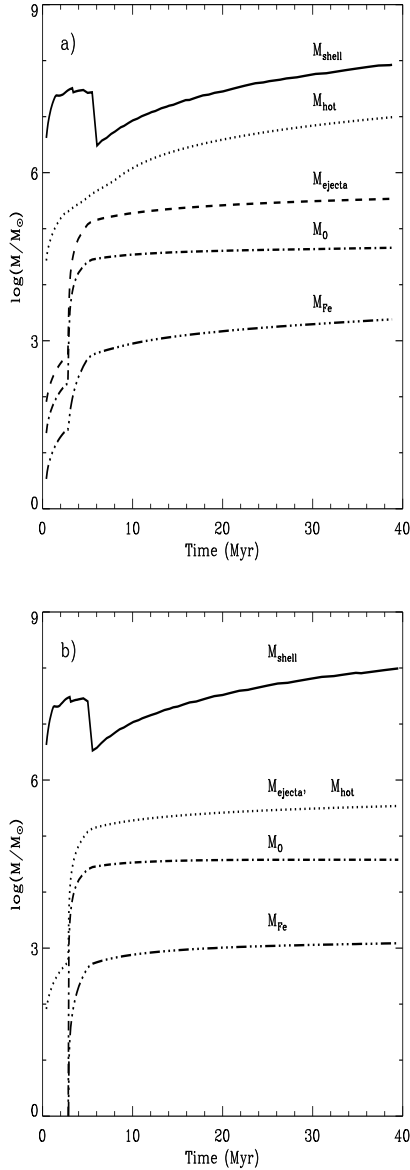


Figure 4. The log of the swept up mass (in M_{\odot}) and that inside the superbubbles for cases 1A (a) and 2A (b), as a function of time. The curves represent the log of: total swept up mass (solid lines), total mass inside the superbubbles (dotted lines labeled M_{hot}). The latter includes both the amount of matter thermally evaporated from the shell (not shown) and the mass ejected by SN (dashed lines labeled M_{ejecta} , coinciding with M_{hot} in panel b). Also shown are the log of the total oxygen and iron mass (dash-dotted lines). In both cases these were calculated following the NW and A approximations (see section 2)

times after the start of the SN phase (3 Myr), a value of Z_O larger than $30 Z_{\odot}$ (case 2A). Even after a substantial fall, as the less massive stars become SN, this case ends with $Z_O \sim 15 Z_{\odot}$ (Figure 5c). In this case $Z_{Fe} \sim 6 Z_{\odot}$ after 6 Myr of evolution and remains almost constant throughout the calculation. Case 2B (under the WW and T assumptions for the metal production rate) presents a rapid rise in Z_O reaching a maximum $Z_O = 8 Z_{\odot}$ at about 10 Myr and then slowly declines to $6 Z_{\odot}$ after 40 Myr. The Z_{Fe} on the other

hand, remains subsolar for the first 12 Myr and then rapidly rises to reach $6 Z_{\odot}$ after 40 Myr (Figure 5d).

For the most energetic starburst (case 3) large values of $Z_O \geq 10 Z_{\odot}$ are found within the first 15 Myr (Figure 5e), when the NW and A metal production rates and $Z_{ISM} = 0.1 Z_{\odot}$ are used (model 3A). The enhanced metallicities however, are not diluted in this case as the fast and hot quasi-adiabatic outer shell has inhibited mass evaporation.

As we increase the initial ISM metallicity from $0.1 Z_{\odot}$ to Z_{\odot} for model 3B, the interior bubble metallicity is lower and more peaked with time (Figure 5f). This unexpected result is produced by a much faster shell cooling, as it is more metal rich, and thus the starburst ejected metals are more efficiently diluted by the evaporated gas from the shell.

Finally, we comment on present day abundance determination of X-ray gas. *ROSAT* observations allow, in principle, for the derivation of metal abundance, of a ($T \sim 1 - 30 \times 10^6$ K) plasma, by X-ray spectral fittings. However, the process is problematic, because of the poor energy resolution of the *ROSAT-PSPC* detector, and the derived ISM metallicities disagree, in many cases, with those deduced from optical observations (Trinchieri *et al.* 1994; Saracco & Ciliegi 1995; Bauer & Bregman 1996). The situation has somewhat improved with the *ASCA* and *BeppeSAX* observations yet the X-ray measurements still suggest significantly sub-solar abundance for Fe combined with somewhat sub-solar abundances for α -elements (Bauer & Bregman 1996, Ptak *et al.* 1999, Persic *et al.* 1998). In some of the cases, the optical observations clearly indicate higher metallicities.

In other words, the complexity of the X-ray spectra of starburst galaxies, combined with the poor spectral resolution of the pre-Chandra and pre-XMM observations, makes the determination of metallicities very model dependent (e.g. Netzer 1999). Dahlem, Weaver & Heckman (1998) and Weaver *et al.* (1999) have discussed the difficulties in deriving metallicities from X-ray data, and, by combining *ROSAT* and *ASCA* data for nearby edge-on starbursts like NGC 253 and M 82, they concluded that the fitting is consistent with near solar abundances and therefore, extremely low metallicities as derived by only *ROSAT* or *ASCA* data are no longer required.

4 THE X-RAY LUMINOSITY OF SUPERBUBBLES

The X-ray emission from superbubbles arise from two different physical regions: the dense outer shell of accelerated ISM and the hot superbubble interior (Suchkov *et al.* 1994, Silich & Tenorio-Tagle 1998, Strickland & Stevens 1998, D'Ercole & Brighenti 1999). Our description of the inner bubble structure is based on the Weaver *et al.* (1977) similarity solution, and assumes that the density n and temperature T profiles can be approximated by

$$n = n_c(1 - x)^{-\lambda}, \quad (12)$$

$$T = T_c(1 - x)^{\lambda}, \quad (13)$$

where n_c and T_c are the central hot gas number density and temperature, and $x = r/R_{sh}$ is the dimensionless distance

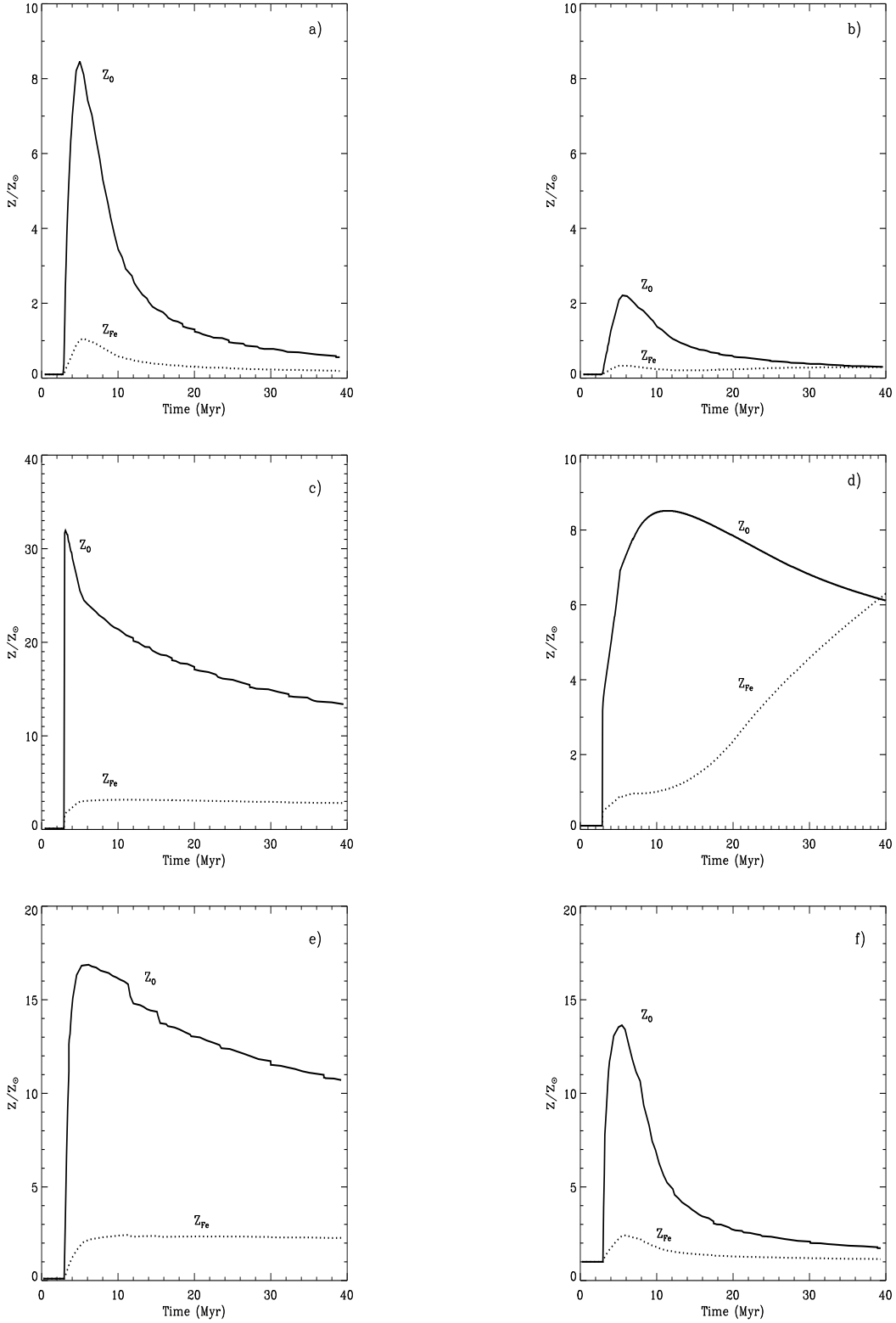


Figure 5. The panels display the oxygen and iron content of superbubbles (in solar units: $Z_O = 0.0083$ and $Z_{Fe} = 0.00126$, from Grevesse and Noels 1996) for the models (a): 1A (with thermal evaporation of the cold outer shell segments) and NW and A approximations; (b) 1B with WW and T approximations; (c) 2A (no mass evaporation, NW and A approximations); (d) 2B, (no mass evaporation, WW and T approximations); (e) 3A, a $10^7 M_{\odot}$ starburst within a $0.1 Z_{\odot}$ ISM, and (f) 3B, a $10^7 M_{\odot}$ starburst within a Z_{\odot} ISM.

from the bubble center. To account for the expected difference in density and temperature distributions for adiabatic and radiative shell segments, we approximate the inner bubble luminosity as

$$L_{x,in} = \epsilon L_R + (1 - \epsilon) L_A \quad (14)$$

where ϵ is the ratio of the radiative surface segments to the total remnant surface area, and L_R and L_A are the X-ray emissions from the interior of the fully radiative and adiabatic bubbles, respectively (Silich & Tenorio-Tagle, 1998)

$$\begin{aligned} L_{x,in} &= \int_0^{2\pi} d\phi \int_0^\pi \sin \theta d\theta \int_0^{R_{cut}} \xi n^2(r) \Lambda_x(T) r^2 dr \\ &= 3\xi \lambda^{-1} n_c^2 \Omega I(T_c, \lambda) \end{aligned} \quad (15)$$

Here $I(T_c, \lambda)$ is a dimensionless integral given by

$$\begin{aligned} I(T_c, \lambda) &= \frac{1}{T_c} \int_{T_{cut}}^{T_c} \Lambda_x(T) \left(\frac{T}{T_c} \right)^{(1-3\lambda)/\lambda} \\ &\quad \left[1 - \left(\frac{T}{T_c} \right)^{1/\lambda} \right]^2 dT, \end{aligned} \quad (16)$$

R_{cut} and T_{cut} are the X-ray cut-off radius and temperature respectively. We used self-similar power index $\lambda = 2/5$ for L_R , and $\lambda = 1/20$ for a more homogeneous gas distribution within a bubble with an adiabatic hot shell. The X-ray luminosity from the adiabatic shell segments is taken to be

$$L_{x,shell} = \xi \sum n_{shock}^2 \Lambda_x(T_{shock}) \Delta R d\Sigma, \quad (17)$$

where $d\Sigma$ is the adiabatic segment surface area, and ΔR is the segment thickness.

Figure 6a shows the total and the shell contribution to the X-ray emissivity of case 1A, using the hot gas metallicities shown in Figure 5a. The contribution of the shell to the total emission becomes most important immediately after blow-out of the remnant from the central gas distribution into the extended halo of the host galaxy. During blow-out the shock reaches speeds of several hundreds of km s^{-1} leading to the high temperatures ($T \sim 1.4 \times 10^7 v_{shock}^2$; where v_{shock} is the shock velocity in units of 10^3 km s^{-1}) which allow the shocked gas to radiate in the X-ray regime. The shell contribution becomes rapidly less important as the shock slows down and the shell cools below the X-ray cut-off temperature ($\sim 5 \times 10^5$) and condenses into a narrow and dense outer boundary of the superbubble. On the other hand, the luminosity of the superbubble interior is found to remain within the range of observed values ($10^{38} - 5 \times 10^{39} \text{ erg s}^{-1}$) throughout the evolution. Figure 6b compares the time dependent X-ray luminosity for our case 1 under the two assumptions for metal production rate. Clearly, the lower metallicities reached in the WW model, lead to a smaller X-ray emission, although the difference never amounts to more than a factor of 5.

Figure 6c gives the contribution to the X-ray luminosity of case 1A in two different energy bands, as a function of time. The two energy bands considered are from 0.1 to 2.2, and from 1.6 to 8.3 keV (X-ray emissivities from Suchkov *et al.* 1994). Clearly, most of the X-ray luminosity arises from the soft X-ray component. The high energy X-rays are due mostly to the larger central temperatures in the superbubble interior.

Figure 7 shows the time evolution of L_X , per unit mass, in models 1A, 2A, 3A and 3B, as well as the same quantity for model A1 from model I which did not include changes in

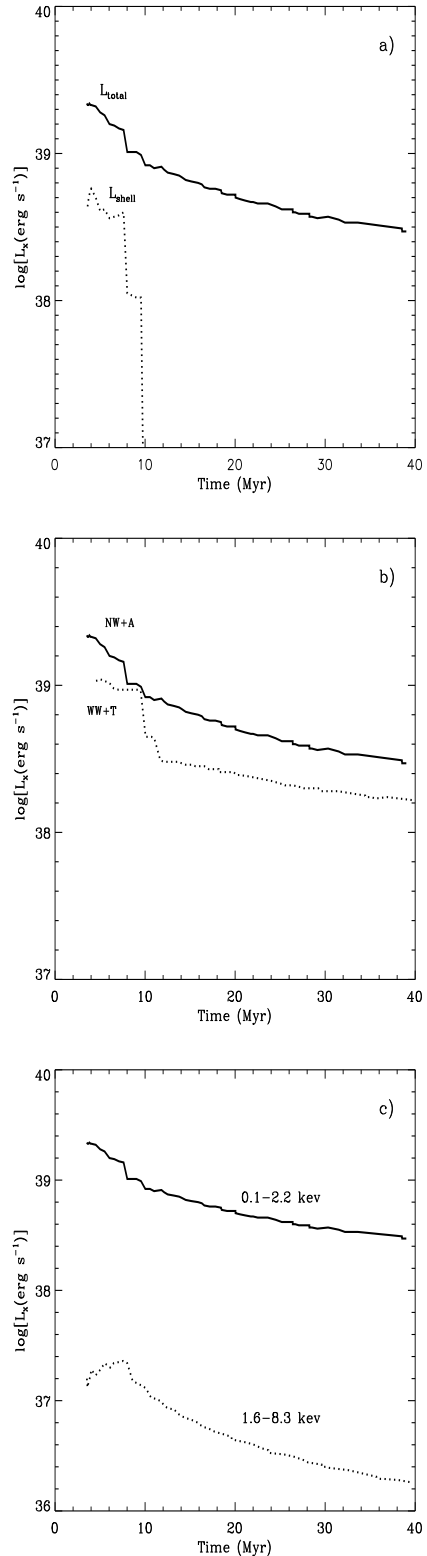


Figure 6. The log X-ray luminosity, as a function of time, for case 1A under NW and A approximations. (a) shows the outer shell contribution (dotted line) and the total luminosity (solid line); (b) compares the above total luminosity with that derived for case 1B under the WW and T assumptions (dotted line); and (c) shows the X-ray luminosity in the two indicated X-ray bands for case 1A.

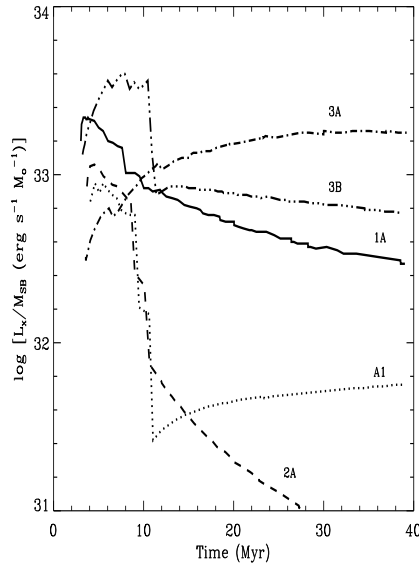


Figure 7. The log of the X-ray luminosity of superbubbles per unit mass as a function of time for cases 1A (low Z), comparison A1 (from paper I) (low Z), 2A (low Z), and massive starburst 3A (low Z) and 3B (solar abundance), as labelled.

metallicity due to the injection of new metals into the cavity. The main difference between case 1A and reference case A1 comes from the hot superbubble interior and can amount to more than an order of magnitude, particularly after 10 Myr, once the shell contribution has become negligible in both cases. Note that the X-ray luminosity of case A1 is in fact rather similar to that of case 2A (without thermal evaporation). However, in case 2 the reduced X-ray emissivity from the interior is due to the fact that, without the substantial extra mass input, the amount of matter able to radiate is orders of magnitude too small. Case 3, our most powerful starburst, leads to the largest luminosities of all cases.

It is interesting to notice an important difference between the bubble evolution in low (case 3A) and high (case 3B) metallicity ISMs. Up to 10 Myr, the X-ray luminosity of the bubble in the metal-rich galaxy is almost an order of magnitude larger than that for the low metallicity one. However, as the high metallicity bubble reaches the radiative phase much earlier than the low metallicity one, the metal-rich shell (3B) cools rapidly around 11 Myr, whereas in the metal-poor case (3A) it remains adiabatic and hot. This results in a rapid decrease of L_x in the high metallicity model, which, after 12 Myr, drops below the X-ray emission from the low metallicity one, and decline more slowly afterwards. The plot indicates that similar X-ray luminosities per unit mass ($\sim 10^{33} \text{ erg s}^{-1} \text{ M}_\odot^{-1}$) arise from cases that allow mass evaporation from the outer shell, irrespective of the mass of the starburst causing the superbubble. This is very different from the calculations that do not account for the change in metallicity of the superbubble interior (case A1, from paper I) and also from those that do not account for mass evaporation (case 2).

5 CONCLUSIONS

The calculations presented here, with the exception of those for the more massive starburst (case 3), differ only slightly in their final outcome regarding the size, expansion velocity and amount of matter swept by evolving superbubbles. However, they show enormous differences in the metallicity of the hot interior, and thus produce largely different X-ray emissivities.

The effects of injection of new metals into the superbubble interior is most noticeable during the HII region lifetime (the first 10 Myr). If oxygen is used as a tracer, the metallicity reaches, immediately after the start of the SN phase, values well above solar metallicity. The maximum value is achieved 3 to 5 Myr after the beginning of this phase. Later, mixing with the evaporated mass slowly reduces the impact of SNe. Note however, that if massive stars are assumed not to have strong winds, large values of $Z \geq Z_\odot$ would remain present inside the superbubble for at least the time required to reach the end of the type II SN phase (40 Myr). This is true even in the extreme case where the host galaxy initial metal abundance is well below solar. On the other hand, if iron is used as the tracer of metallicity, values of $Z_{Fe} \leq Z_\odot$ are always predicted, regardless of the assumed iron production scheme. The above results are to be compared to the cases without mass evaporation, all of which led to metallicities larger than solar throughout the evolution, regardless of the assumed tracer.

More massive starbursts result in very strong shocks and longlasting hot, quasi-adiabatic outer shell from which thermal evaporation is strongly inhibited. Such starbursts show over solar metallicity throughout their evolution, regardless of the assumed tracer.

The most important conclusion is that enhanced metallicity of superbubble interiors can strongly influence their X-ray luminosity, bringing theory and observations into a better agreement.

6 ACKNOWLEDGMENTS

The authors acknowledge fruitful conversations with Andy Fabian, and with Dahlem and Weaver, who kindly provided us with their results prior to publication.

SAS acknowledges support from a Royal Society grant for joint projects with countries of the former Soviet Union. SAS, GTT and ET also thank the IoA in Cambridge for their support and hospitality during a visit to the United Kingdom where the calculations were performed. HN acknowledges the hospitality of the IoA Cambridge, where this collaboration was initiated, and financial support by the Israel Science Foundation. Research Grants from CONACYT (Mexican Research Council) are thankfully acknowledged by GTT and ET.

REFERENCES

- Arnett, D. 1991, in *Frontiers of Stellar Evolution*, ed. D.L. Lambert (ASP Conf. Ser., 20), 389
- Bauer, F. & Bregman, J.N. 1996, *ApJ*, 457, 382
- Bisnovatyi-Kogan, G.S. & Silich, S.A. 1995, *Rev. Mod. Phys.* 67, 661

Brinks, E. & Bajaja, E. 1986, A&A 169, 14

Chiosi, C., Nasi, E. & Sreenivasan, S.P. 1978, A&A, 63, 103

Chu, Y.-H., & Mac Low, M.-M. 1990, ApJ, 365, 510

Dahlem, M., Weaver, K.A. & Heckman, T.M. 1998, ApJ Suppl. Ser., 118, 401

D'Ercole, A. & Brighenti, F. 1999, astro-ph/9907005

Franco, J., Ferrara, A., Rozyczka, M., Tenorio-Tagle, G. & Cox, D.P. 1993, ApJ, 407, 100

Heckman, T.M., Armus, L. & Miley, G.K. 1990, ApJ Suppl. Ser. 74, 833

Heckman, T.M., Dahlem, M., Eales, S.A., Fabbiano, G., Weaver, K. 1996, ApJ, 457, 616

Heckman, T.M., Dahlem, M., Lehnert, M.D., Fabbiano, G., Gilmore, D. & Waller, W.H. 1995, ApJ, 448, 98

Heiles, C. 1979, ApJ, 229, 533

Grevesse, N., Noels, A. & Sauval, A.J. 1996, ASP Conf. Ser., eds. Holt, S.S. & Sonneborn, G. 99, 117

Li, F. & Ikeuchi, S. 1992, ApJ 390, 405

Leitherer, C. & Heckman, T.M. 1995, ApJS, 96, 9

Martin, C.L. & Kennicutt, R.C. 1995, ApJ, 447, 171

Martin, C.L. 1996, ApJ, 465, 680

Maeder, A. 1992, A&A, 264, 105

Maschenko, S., Thilker, D. & Broun, R. 1999, A&A, 343, 352

Meaburn, J. 1980, MNRAS, 192, 365

Netzer, H., 1999, Astron.Nach., 4/5, 171

Oey, M.S. 1996, ApJ, 467, 666

Persic, M., Mariani, S., Cappi, M., Bassani, L., Danese, L., Dean, A.J., Di Cocco, G., Franceschini, A., Hunt, L.K., Matteucci, F., Palazzi, E., Palumbo, G.G.C., Rephaeli, Y., Salucci, P. & Spizzichino, A., 1998, A&A, 339, L33

Pilyugin, L.S. 1993, A&A, 277, 42

Pilyugin, L.S. & Edmunds, M.G. 1996, A&A, 313, 792

Ptak, A., Serlemitsos, P., Yaqoob, T. & Mushotzky, R. 1999, ApJS, 120, 179

Renzini, A., Ciotti, L., D'Ercole, A. & Pellegrini, S. 1993, ApJ, 419, 52

Silich, S. 1995, Astron. and Astroph. Transactions, 9, 85

Silich, S. & Tenorio-Tagle, G. 1998, MNRAS, 299, 249

Stothers, R. 1972, ApJ, 175, 431

Strickland, D.K. & Stevens, I.R. 1998, MNRAS, 297, 747

Suchkov, A., Balsara, D., Heckman, T. & Leitherer, C. 1994, ApJ 430, 511

Tenorio-Tagle, G. 1996, AJ, 111, 1641

Tenorio-Tagle, G. & Bodenheimer, P. 1988, ARA&A 26, 145

Tenorio-Tagle, G. & Muñoz-Tuñón, C. 1998, 293, 299

Tenorio-Tagle, G., Silich, S., Kunth, D., Terlevich, E. & Terlevich, R.: 1999, MNRAS, 309, 332

Thielemann, F.-K., Nomoto, K., Shigeyama, T., Tsujimoto, T. & Hashimoto, M. 1992, in Elements and the Cosmos, Eds. R. J. Terlevich, B. Pagel, R. Carswell & M. Edmunds Cambridge University Press, 68

Thielemann, F.-K., Nomoto, K. & Hashimoto, M. 1993, in Origin and Evolution of the Elements, Eds. N. Prantzon, E. Vangioni-Flan, M. Casse Cambridge University Press, 297

Trinchieri, G., Kim, D.-W., Fabbiano, G. & Canizares, C. R. C. 1994, ApJ 428, 555

Tomisaka, K. & Bregman, J.N. 1993, PASJ, 45, 513

Walter, F., Kerp, J., Duric, N., Brinks, E. & Klein, U. 1998, ApJ Letters, 502, L143

Wang, Q.D. & Helfand, D. 1991, ApJ, 379, 327

Wang, Q.D. 1999, ApJ Letters, 510, L39

Weaver, K.A., Heckman, T. & Dahlem, M., 1999, astro-ph/9911446

Woosley, S.E., Langer, N. & Weaver, T.A. 1993, ApJ, 411, 823